Exp Fluids (2009) 46:1139–1157
DOI 10.1007/s00348-009-0622-9

RESEARCH ARTICLE

An experimental study on jets issuing from elliptic inclined nozzles

T. H. New

Received: 30 August 2008 / Revised: 14 January 2009 / Accepted: 20 January 2009 / Published online: 15 February 2009

Abstract This paper reports on an experimental flow visualisation and digital particle image velocimetry investigation on forced jets exhausting from aspect ratio equal to three elliptic nozzles with exits inclined at 30° and 60°. Flow images show that shear layer instabilities and subsequent vortex roll-ups are formed parallel to the inclined nozzle exits at 30° incline and that rapid re-orientation of the vortex roll-ups occurs at 60° incline. Flow observations also show that strong axis-switching occurs in a non-inclined elliptic nozzle. However, 30° and 60° elliptic inclined nozzles produce significant distortions to and suppression of the axis-switching behaviour, respectively. As a result, flow stresses and turbulent kinetic energy distributions become increasingly asymmetric. Their coherency and magnitudes along the shorter nozzle lengths also vary significantly. This can be attributed to the dissimilar formations of vortex roll-ups and rib structures, as well as unequal mutual interactions between them as the incline-angle increases. Lastly, results also show that unlike circular inclined nozzles, elliptic inclined nozzles do not produce serpentine-shaped jet columns nor lead to significant lateral jet-spread at large incline-angles.

List of symbols

D	Particle diameter
D_h	Hydraulic diameter of elliptic nozzle
D_{major}	Major diameter of elliptic nozzle
D_{minor}	Minor diameter of elliptic nozzle
f	Forcing frequency
H	Nozzle mean height
U_{cl}	Local centerline velocity in the streamwise direction
U_e	Mean jet exit velocity
U_f	Forcing amplitude
U_m	Mean jet velocity
u'	Streamwise velocity fluctuation
v'	Cross-stream velocity fluctuation
$u'u'$	Streamwise flow stress
$u'v'$	Reynolds shear stress
$v'v'$	Cross-stream flow stress
x	Streamwise distance from nozzle mean height
y	Cross-stream distance from nozzle center
δ	Jet exit shear layer thickness
ρ	Particle density
$\tau_{particle}$	Particle time scale $\tau_{particle} = \rho D^2/18\mu$
τ_{flow}	Jet flow time scale $\tau_{flow} = \delta/U_{cl}$
μ	Dynamic viscosity of water
ν	Kinematic viscosity of water
Re	Reynolds number $Re = U_e D_h/\nu$
St	Strouhal number $St = fD_h/U_e$
Stk	Stokes number $Stk = \tau_{particle}/\tau_{flow}$
AR	Aspect ratio
DPIV	Digital particle image velocimetry
Px	Pixel

1 Introduction

The study of elliptic jets is a well-established one, with notable investigations carried out over the past years by researchers working in the area of jet-mixing enhancement and/or control techniques. One of the earliest studies on the

T. H. New (✉)
Department of Engineering, University of Liverpool,
Liverpool L69 3GH, UK
e-mail: T.New@liverpool.ac.uk

use of elliptic jets to manipulate jet-mixing behaviour was carried out by Crighton (1973) on their stability analysis. In that study, it was suggested that the differing behaviour in the growth rates along the major- and minor-planes of the elliptic jet may be used to silent jets. Further studies were made by Husain and Hussain (1983) when they studied both unexcited and excited elliptic jets. They found that the axis-switching locations and associated flow characteristics can be manipulated significantly by flow excitations. Axis-switching in elliptic jets occurs when its major- and minor-axes interchange as they convect downstream. Higher self-induced velocities in the initial elliptic vortex filament portions at the major-plane ends will cause them to accelerate downstream and towards the jet centerline. On the other hand, filament portions at the minor-plane ends will slow down and move away from the jet centerline. The net effect is a decrease and increase in the major- and minor axis lengths, respectively, such that the axes rotate and "switch" with each other. Depending on the exact flow conditions, axis-switching events may repeat until transition to turbulence occurs.

On the other hand, Gutmark and Ho (1985) surveyed the fluctuating pressure fields resulting from the use of an aspect ratio (AR) AR = 2 elliptic jet. They observed little differences in the results obtained along the major- and minor-planes. They followed up with another study (Gutmark and Ho 1986) where they found evidences of strong axis-switching consistent with earlier studies using flow visualisations. Later, Ho and Gutmark (1987) ascertained the entrainment of an AR = 2 elliptic jet and determined it to be much higher than a typical round jet. The study also revealed that the elliptic jet initial instability mode is strongly linked to the thinnest jet momentum thickness within their non-uniform distribution around the elliptic jet circumference. This was later supported by a numerical investigation carried out by Morris (1988). Hussain and Husain (1989) and Husain and Hussain (1991, 1993) carried out an extensive series of experiments on the behaviour of coherent structures in elliptic jets. They are found to be strongly affected by initial flow conditions, i.e. jet aspect ratio, initial momentum thickness, unexcited and excited flows, among others. Their studies also showed that the resultant flow behaviour is closely linked to the distribution of the initial momentum thickness. By manipulating that distribution, they were able to induce a range of different vortical behaviour. Particularly interesting within the same study is the bifurcation of a high aspect ratio elliptic jet (AR = 4) at sufficiently high excitation amplitudes and the flow mechanisms underpinning the bifurcation, as it illustrates the extent of flow control possibilities using elliptic jets. The pairing process of elliptic jets was also observed to be significantly different from that of circular jets due to the continuously evolving curvature and outline of the vortex roll-ups. The result is a highly localised and three-dimensional vortex entanglement process before merging of the vortex roll-ups occurs. Other coherent flow structures such as the streamwise-aligned vortices (or ribs) were also found to contribute significantly towards the entrainment ability of elliptic jets and the mechanisms of their formation and interactions with the vortex roll-ups were clarified.

The sensitivity of elliptic jets towards the distribution and thickness of the momentum thickness can also be observed in studies carried out by Schadow et al. (1987), Quinn (1989) and Lee and Baek (1994). Occurrence of axis-switching, axis-switching locations and entrainment rates have been found to differ between elliptic jets of different aspect ratios produced via different means. Elliptic jets produced from orifices, straight pipes and contoured apparatuses tend to possess very different momentum thickness distributions and hence, directly impact upon the flow behaviour. The wide range of behaviour demonstrated by elliptic jets has also lead to studies utilising it for high-speed flows and other flow control techniques. For instance, Kinzie and McLaughlin (1999), Tam and Pastouchenko (2002) evaluated jet noise from elliptic jets operating at subsonic and supersonic speeds, while Husain and Hussain (1999) studied whistler jets making use of elliptic geometries. Together with the earlier studies, these investigations show that there remains a host of possibilities to exploit the unique elliptic geometry further for passive mixing and control gains. Hence, these considerations provide one of the primary motivations for the present study.

On the other hand, the study of jets issuing from simple inclined nozzles remains comparatively limited with most studies focusing their efforts on the use of circular nozzle geometry. For instance, Wlezien and Kibens (1986) studied inclined nozzles as part of a wider investigation involving indeterminate-origin jets. They observed that modifications to the circumferential energy distribution within the jet shear layers are possible and that inclined nozzles promote self-excitations of the resultant jet flows. A more recent study by Webster and Longmire (1997) on jets discharging from inclined nozzles further revealed that under forced flow conditions, the inclined vortex roll-ups will undergo pairing provided that the incline-angle remains moderate. When the incline-angle becomes large and coupled with relatively higher forcing frequencies, the pairing process will be suppressed due to faster breaking down of the vortex roll-ups.

A closely related study focusing on the influence of the inclined nozzle exits on the production of vortex rings was later carried out by the same authors (Webster and Longmire 1998). It was observed that the resultant vortex rings possess non-uniform circulation along their circumferences

which causes them to move away from the nozzle centerline and towards the shorter nozzle length. These are in-line with observations from their earlier study using forced jets. Lim (1998) also carried out a series of experiments on vortex rings issuing from inclined nozzles. The study showed that depending on the incline-angle, Reynolds number and the stroke length, circumferential flows along the vortex ring filaments may lead to breakdowns of or "bulging"-like behaviour in the vortex cores. Hence, the stability of vortex rings or vortex roll-ups produced from inclined nozzles can be significantly reduced not only by the initial geometric conditions, but through more localised but associated flow events as well.

While considerable insights have been gathered from the above studies on inclined nozzles, there remains a lack of good understanding on inclined nozzles which make use of noncircular geometries. Hence, the present study seeks to investigate elliptic nozzles with inclined exits, i.e. elliptic inclined nozzles, which complement the main objective of manipulating conventional elliptic jet flows further. The elliptic nozzle geometry represents an ideal first step towards understanding the use of other noncircular geometries as it typically possesses smooth variations of circumferential momentum thickness due to its lack of sharp corners, as compared to other noncircular geometries. Furthermore, the behaviour of conventional elliptic jets is relatively well-understood, given the extent of studies dedicated to their elucidation as outlined earlier. Hence, current knowledge on elliptic jets can be leveraged upon to extend to the case of inclined nozzles. In particular, it is of significant interest to study if the coherent axis-switching behaviour in elliptic jets can be altered by manipulating the elliptic nozzle geometry. Since axis-switching behaviour in elliptic jets typically commences with distinct and strong bending of the elliptic vortex filament along its major-plane towards the downstream direction, implementing inclined exits along the nozzle major-planes are likely to have more significant effects. Furthermore, by increasing the incline-angle of the inclined exits along the major-planes systematically, any alterations to the axis-switching behaviour caused by the increasingly inclined vortex roll-ups along the major-planes can be deduced logically. While imposing inclined exits along the minor-planes is also likely to lead to other unique flow effects, the present configurations will nonetheless be a useful first step towards understanding elliptic inclined nozzles in general.

Hence, the present study made use of flow visualisation and digital particle image velocimetry (DPIV) techniques to investigate the effects of imposing inclined exits with different incline-angles on AR = 3 elliptic nozzles along the major-planes. The results will be compared with a benchmark conventional non-inclined elliptic nozzle of similar aspect ratio. To ensure that the large-scale vortex roll-ups are formed according to the contours of the inclined elliptic nozzle exits, as well as better organising the dominant vortex structures in the resultant flow fields, forcing at a fixed frequency was used in the present study. Furthermore, the aspect ratio of the elliptic nozzle and experimental procedures are carefully selected such that the resultant jet flows are not likely to bifurcate. For example, Hussain and Husain (1989) observed bifurcations of an AR = 4 elliptic jet under significant forcing. Therefore, the aspect-ratio of the elliptic nozzle used here was restricted to AR = 3 and forcing amplitude used was substantially lower than the minimum level that would lead to jet bifurcations.

Information on the experimental setup and procedures will be provided in the next section, followed by detailed qualitative and quantitative descriptions on the near-field vortex dynamics. Special attention will be paid towards the effects of the inclined nozzles on the inherent axis-switching behaviour and mixing characteristics observed in conventional elliptic jets. Lastly, a brief conclusion will then be provided to summarise the main findings in this study.

2 Experimental setup and procedures

2.1 Experimental apparatus and nozzle designs

All flow visualisation and DPIV experiments were carried out in the Department of Engineering at the University of Liverpool. A recirculating nozzle-testing water-tank with internal dimensions of 400 mm (W) × 400 mm (H) × 800 mm (L) was used for the experiments as shown in Fig. 1. A centrifugal pump channeled water from a small water reservoir through a Blue-White Industries F-400 rotameter which was calibrated against a Fischer and Porter 10DS4111 electromagnetic flow meter before the experiments. The water subsequently entered a jet apparatus consisting of a diffuser, flow-straightening honeycombs, three layers of fine-screens for turbulence reduction and a contoured circular-to-elliptic contraction chamber. The profile of the circular-to-elliptic contraction chamber used in this study was based on fifth-order polynomial curves along both the major and minor-axes with smooth transitions between them. The contraction ratio used was 22:1. The flow-conditioned water would then exhaust out into the quiescent water tank thereafter via the attached test nozzle. Any water overflow would be captured by two overflow PVC pipes at the end of the water tank and redirected back into the small water reservoir to complete the flow circuit. The test nozzles are attached to the jet apparatus via eight equally spaced screw locations and they

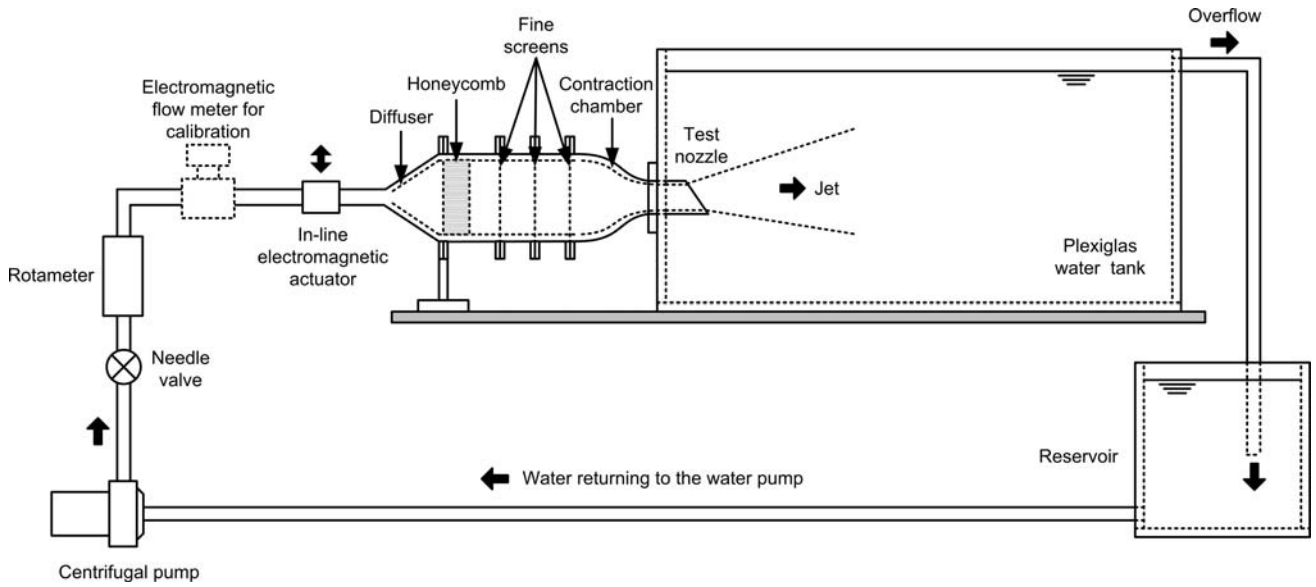

Fig. 1 Schematics of the recirculating water-tank and associated experimental setup

are rotated 90° for major- or minor-plane alignments during the experiments.

Three AR = 3 elliptic nozzles are investigated in the present study and Fig. 2 shows their design schematics and reference coordinates. In addition to the benchmark elliptic reference nozzle, two elliptic inclined nozzles with incline-angles of 30° and 60° with respect to the vertical along the major-plane are used. The major- and minor-axes of all the elliptic nozzles measure $D_{\text{major}} = 36.7$ mm and $D_{\text{minor}} = 12.3$ mm, respectively, which yields a hydraulic diameter of $D_{\text{h}} = 16.4$ mm throughout. The distances from the nozzle bases to their origins (or nozzle mean height) are also maintained at a consistent 40 mm ($H/D_{\text{h}} = 2.4$) for all nozzles as indicated by the figure. All elliptic nozzles were fabricated from brass with their wall thicknesses kept at 1 mm throughout the nozzle circumferences. Mean jet velocity was maintained at $U_{\text{e}} = 0.15$ m/s with a resultant Reynolds number of approximately $Re = 2{,}500$.

The study was carried out under forced conditions where a LDS Ltd V201/3 electromagnetic actuator driven piston setup was used to impart regular perturbations to the jet flows with an estimated amplitude of $U_{\text{f}} = 0.02U_{\text{e}}$ at a frequency of $f = 4.6$ Hz (or Strouhal number of $St = 0.5$ based on the hydraulic diameter). The forcing amplitude was estimated using time-sequenced DPIV measurements taken at 15 Hz by determining the maximum velocity increase in the average jet exit velocity caused by the forcing, using unforced jet flow as a comparison. By evaluating the phase information of the DPIV measurements and the forcing, the maximum uncertainty in the estimated forcing amplitude was evaluated to be approximately $\pm 0.004U_{\text{e}}$. The electromagnetic actuator was used to drive a piston as the forcing device to perturb the jet flows and relatively similar to the technique used successfully by Longmire and Duong (1996), Webster and Longmire (1997) and New et al. (2005). For the sake of brevity here, readers are advised to refer to their studies for more details on the forcing technique. A TTi TG315 waveform generator was used to generate square-wave signals which were channeled to a LDS Ltd PA100 power amplifier connected to the electromagnetic actuator. The amplification level was adjusted such that the forcing amplitude was just sufficiently strong to produce regular vortex roll-ups without grossly distorting the dominant flow features. This ensured that the vortex roll-ups followed the entire nozzle exit lip contours to allow consistent comparisons.

2.2 Flow visualisation and DPIV setup

Flow visualisation was carried out by controlled release of coloured-dye circumferentially into the jet shear layer using a gravity-feed technique as shown in Fig. 3. The coloured-dye entered the dye-injection apparatus via four evenly spaced (i.e. 90° apart) 3 mm diameter ports into a cylindrical dye port within the jet apparatus. As the jet fluid travelled from the contraction chamber and into the nozzle via the dye-injection apparatus, coloured-dye would be evenly released into the entire shear layer through a 1 mm thick circumferential slit. The slit was located 59 mm upstream of the nozzle origin. A 500 W halogen floodlight was used to illuminate the resulting jet flows and a 3CCD colour video camera was used to capture the resultant flow structures at 25 frames per second. Still images were then extracted from the recorded

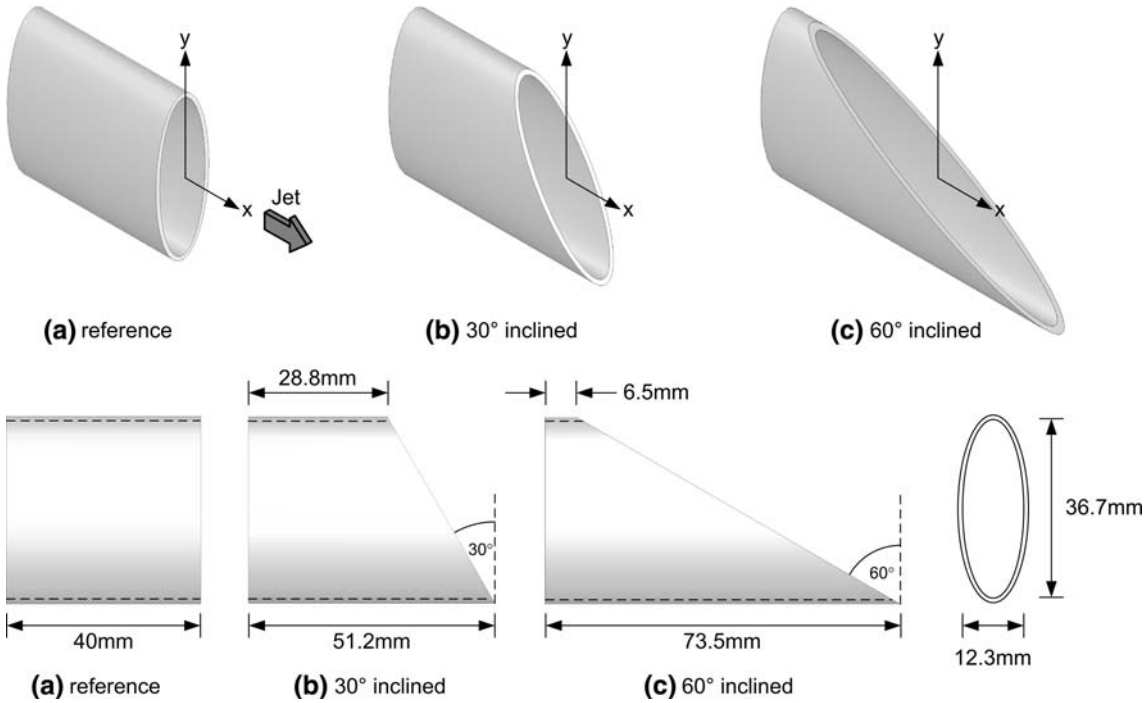

Fig. 2 Schematics of the three elliptic nozzles used in the present study, which include the **a** elliptic reference, **b** 30° and **c** 60° elliptic inclined nozzles

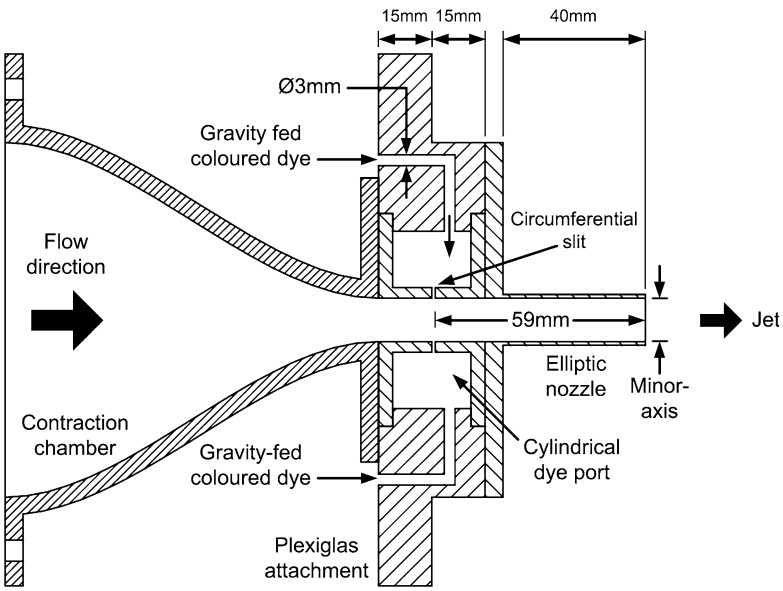

Fig. 3 Cross-sectional view of the circumferential dye-injection apparatus

videos on a workstation for subsequent analysis. DPIV measurements were facilitated by a 2D Dantec DC-Imaging PIV system capable of operating in double-frame mode at 15 Hz. The illumination source was a New Wave Research Minilase 50 mJ double-pulsed Nd:YAG laser operating at 532 nm wavelength, where the laser beams were expanded to form thin laser sheets using beam-expanding optics. During the experiments, the laser sheet thickness was limited to approximately 1 mm by using slits before they transmitted through the Plexiglas water tank. Fifty micron diameter polyamid seeding particles of specific gravity of 1.03 g/cm^3 were used to seed both the water tank and jets uniformly to ensure good distributions during experiments. An 8-bit 1600px by 1200px grayscale FlowSense CCD camera with a Nikon 60 mm f2.8 lens were used to capture image-pairs of scattered light from the particles.

The ability of the seeding particles to track the jet flows was evaluated by determining the Stokes number (*Stk*). It is

defined here as $Stk = \tau_{particle}/\tau_{flow}$ where $\tau_{particle}$ and τ_{flow} are the particle and jet flow time scales, respectively. To calculate the particle time scale, $\tau_{particle} = \rho D^2/18\mu$ was used where ρ and D are the particle density and diameter, respectively and μ is the water dynamic viscosity. On the other hand, the jet flow time scale was determined using $\tau_{flow} = \delta/U_{cl}$, where δ and U_{cl} are the jet exit shear layer thickness and local centerline velocity in the streamwise direction, respectively. Based on the experimental conditions, the Stokes number was evaluated to be approximately $Stk = 0.0014$ and well within the acceptable limit as indicated by Crowe et al. (1988).

All DPIV experiments were carried out at full 15 Hz with the time-interval between images within an image-pair kept at 2 millisecond throughout. As the present study focus on the time-averaged flow behaviour under forced conditions, the DPIV experiments were carried out without any preference to any particular phase of the flow field. A total of 500 image-pairs were captured for each test case and they were evaluated using Dantec FlowManager software using two-pass multi-grid cross-correlations. The initial and final interrogation window sizes are 128 px by 128 px and 32 px by 32 px, respectively with 50% overlap in both directions. The raw velocity vector maps were then subjected to global validation schemes (i.e. peak and moving-average validations) to eliminate erroneous vectors. Lastly, a three-point by three-point neighbourhood moving-average smoothing filter was used to yield the final vector maps and associated vorticity maps. Uncertainty analysis based on Keane and Adrian (1992) indicates that the errors of the determined velocity vectors are within $\pm 1\%$ of the actual velocity components, with an overall accuracy of above 95%.

3 Results and discussions

3.1 Near-field flow characteristics

Figure 4 shows instantaneous dye-visualisation flow images taken of the three elliptic nozzles along the major- and minor-planes. For the elliptic reference nozzle, the presence of axis-switching behaviour in the near-field vortex dynamics can be observed clearly in Fig. 4a and d. This behaviour is reminiscent of earlier experimental evidences presented by Gutmark and Ho (1986), Ho and Gutmark (1987) and Hussain and Husain (1989). This is despite the fact that different elliptic jet aspect-ratios were used in these earlier studies, and that nozzles are used here instead of jet exits flushed with the tank wall surfaces. Under the actions of forcing, shear layer instabilities formed readily around the circumference of the jet shear layer. Note that the forcing frequency was intentionally selected to be close to the preferred mode for elliptic jets (approximately $St = 0.4$) as observed by Hussain and Husain (1989), which would not lead to pairing of the vortex roll-ups and thus ease flow observations. Furthermore, the forcing amplitude was also significantly lower than the level observed to cause jet bifurcation for an AR = 4 elliptic jet (approximately 5% of the jet exit velocity minimum as indicated by Hussain and Husain (1989)). Hence, jet bifurcation behaviour is not expected to manifest here as well.

Rolling-up of the elliptic shear layer occurs along regions where the radii of curvature are maximum, i.e. at the minor-plane ends, before the process propagates along the filament symmetrically towards regions where radii of curvature are minimum, i.e. at the major-plane ends. According to observations made by Ho and Gutmark (1987) and Hussain and Husain (1989), this indicates that the momentum thickness along the minor-plane is discernibly smaller than that along the major-plane. Thereafter, the major-axis regions of the elliptic vortex roll-up will accelerate past the minor-axis regions of the same elliptic vortex roll-up in the downstream direction due to higher self-induced velocities. Concurrently, they also move laterally inwards and towards the nozzle centerline. The effects of this will lead to increase in self-induced velocities in the minor-axis regions of the elliptic vortex roll-up as well, which sees them moving laterally outwards. As a result, the overall extent of the vortex roll-up major-axis will reduce while that along the minor-axis will increase as depicted in Fig. 4a and d. For the present flow conditions, only one-cycle of axis-switching can be observed before rapid transition to a turbulent state occurs.

When the jet was exhausted from the 30° elliptic inclined nozzle instead as shown in Fig. 4b and e, it can be seen that the original axis-switching behaviour in the reference test case has been altered. Upon each forcing cycle, distinct elliptic shear layer instability and subsequent vortex roll-up inclined parallel to the nozzle exit are consistently formed. This observation is similar to those made by Wlezien and Kibens (1986) and Webster and Longmire (1997) in their studies on circular nozzles with moderate incline-angles. However, unlike these earlier studies, the elliptic vortex roll-up here possesses inherent differences in the self-induced velocities along the vortex roll-up circumference, albeit with different distribution as compared to the elliptic reference case. While rolling-up of the jet shear layer still begins along the minor-plane, it will propagate faster towards the shorter nozzle length than the longer nozzle length. Hence, the vortex roll-up along the major-plane is more developed along the shorter nozzle length than along the longer nozzle length. As the flow convects further downstream, the elliptic vortex roll-up will begin to bend and appear to undergo a limited form of

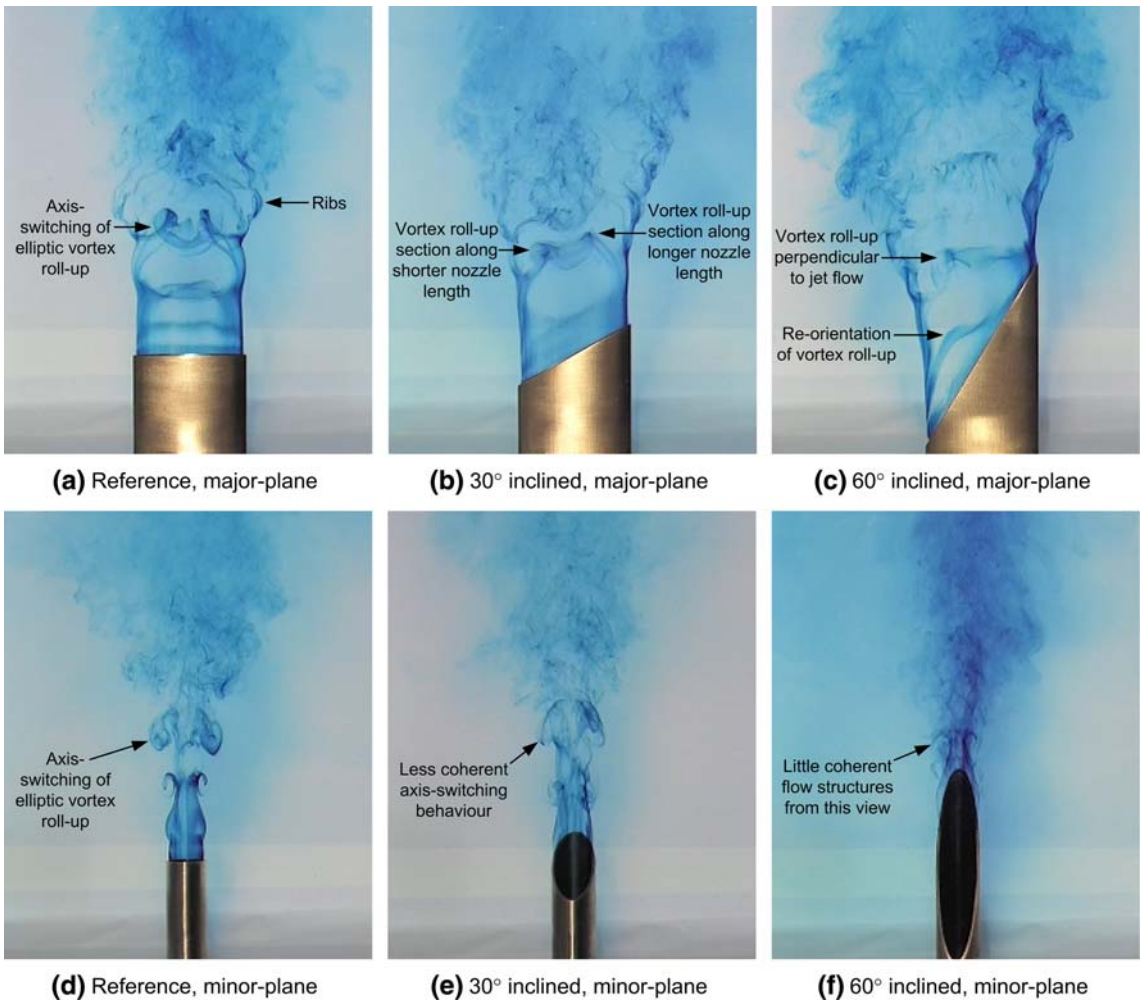

Fig. 4 Instantaneous flow visualisation images captured for the three elliptic nozzles along major- and minor-planes

axis-switching. Figure 4b reveals that the outline of the bending elliptic vortex roll-up share certain similarities to an intermediate state of axis-switching behaviour. In this case however, the overall inclination of the bending elliptic vortex roll-up remains approximately parallel to the inclined nozzle exit. On the other hand, Fig. 4e depicts a much more intense flow field without clear indications of axis-switching behaviour. If axis-switching behaviour was present, the minor-axis regions of the vortex roll-up would be moving laterally outwards and away from the nozzle centerline from this view. Hence, it can be seen that the use of a moderately inclined elliptic nozzle essentially distorts the axis-switching behaviour.

Lastly, Fig. 4c and f show flow images taken for the 60° elliptic inclined nozzle along the major- and minor-planes, respectively. At 60°, the incline-angle should no longer be considered as moderate but substantial instead. As opposed to what was observed in Fig. 4a and b, Fig. 4c shows that the shear layer instabilities are formed parallel to the nozzle exit contour within a short distance away from the nozzle exit. However, they manifest into distinct vortex roll-ups very shortly thereafter with sharp reductions in their inclinations. Furthermore, the initiation of the shear layer roll-up in this case does not appear to be associated with the minor-axis of this particular elliptic nozzle but along the shorter nozzle length region instead. These observations agree well with the experimental results by Wlezien and Kibens (1986) and Webster and Longmire (1997) when they used inclined nozzles of large incline-angles. Similarly, the shear layer roll-up process gradually travels from the shorter nozzle length towards the longer nozzle length.

Clearly, the steepness of the 60° elliptic inclined nozzle meant that the major-axis vortex roll-up at the shorter nozzle length will be even more developed than the case for the 30° elliptic inclined nozzle. In this case, it develops significantly before its counterpart at the longer nozzle length fully forms and accelerates downstream thereafter. This flow acceleration results in the abrupt turning of the inclined elliptic vortex roll-up such that part of it becomes perpendicular to the jet flow direction as shown in Fig. 4c.

Note that at this point, the vortex roll-up at the longer nozzle length has yet to be fully formed until shortly after the turning of the vortex roll-up, where it initiates and surges towards to the nozzle centerline. With that, the entire vortex roll-up convects downstream without any visual evidence of axis-switching detected. It is worth noticing that the general outline of the jet column along the major-plane is skewed towards the shorter nozzle length. As for the view along the minor-plane as shown in Fig. 4f, the visualised flow field is too intense to observe any distinct flow dynamics. However, compared to Fig. 4d and e, the jet column in the case seems to be the narrowest and reinforce the notion that axis-switching has been suppressed.

Based on the flow images presented, the extent to which axis-switching is distorted or suppressed depends very much on the incline-angle. This is not very surprising as it has shown in previous studies (Wlezien and Kibens 1986) that the inclined nozzle exit confers redistributive effects on the azimuthal shear layer energy levels. Furthermore, the presence of axis-switching depends very much on the azimuthal distribution of the momentum thickness. Schadow et al. (1987) and Ho and Gutmark (1987) had shown non-occurrence of axis-switching behaviour in straight elliptic pipes but presence of strong axis-switching behaviour in contoured elliptic nozzles. These studies essentially show that relatively thick jet momentum thickness suppresses axis-switching, while thinner jet momentum thickness and larger discrepancy between the momentum thicknesses along the major- and minor-planes leads to more robust axis-switching behaviour.

In the case of the inclined nozzles used here, it is logical that the momentum thicknesses along the shorter nozzle lengths will be thinner than those along the longer nozzle lengths, since the flow images show them to develop before their counterparts along the longer nozzle lengths. Hence, the vortex roll-up regions along the shorter nozzle lengths will retain the ability to accelerate and behave in an axis-switching like manner. On the other hand, the ability of their counterparts at the longer nozzle lengths to behave in a similar fashion will be significantly limited due to the thicker momentum thickness. In fact, due to the common mean height used in the present study, the tendency for the vortex roll-up portions along the shorter nozzle length regions to undergo axis-switching should be greater than the reference nozzle. Judging from the observations made in Fig. 4 so far, the visual evidences agree well with these considerations.

It has been mentioned earlier on that in a study carried out by Lim (1998) on discrete vortex rings discharging from circular inclined nozzles, breakdown or bulging of the vortex rings was observed, depending on the exact Reynolds number and stroke length. However, no clear observations of such breakdowns are made during the present study, even though some distortions to the vortex roll-ups are apparent. For the vortex ring breakdown or bulging to occur, circumferential flow along the vortex roll-up due to vortex-stretching is required as pointed out by Lim (1998). However, the required extent of circumferential flow remains unknown. In the present study, imposing inclinations on the AR = 3 elliptic nozzle geometry result in flow fields which are dominated by self-induced velocities. Hence, the extent of circumferential flow along the vortex roll-ups will be limited. Furthermore, flow images show vortex roll-ups of the reference and 30° inclined nozzles initiate along the minor-planes before propagating towards the major-planes. This observation indicates higher initial strain rates along the minor-planes. Thus, this is in contrast with the observations made by Lim (1998) that higher strain rates due to vortex-stretching associated with the longer nozzle lengths are driving the circumferential flow along the vortex ring circumference towards the shorter nozzle lengths, and hence the breakdown process.

Additionally, the vortex rings in that study were produced from a straight pipe with uniform velocity profiles which yielded little circumferential momentum thickness variation even for inclined nozzles, as compared to the inclined AR = 3 elliptic jets produced via contoured nozzle apparatus used here. To complicate matters, the inclined elliptic vortex roll-ups here are produced regularly by forcing the flow. Mutual interactions between adjacent vortex roll-ups will further distort the overall vortex dynamics such that their behaviour will deviate from the case of a discrete vortex ring. Nonetheless, the study by Lim (1998) raises interesting questions on the possible existence of the breakdown or bulging process in discrete elliptic inclined vortex rings under suitable conditions.

Lastly, the formation of streamwise-oriented vortices (or Bernal-Roshko vortices, as studied by Bernal and Roshko (1986)) along the peripheral regions of the major-planes can also be consistently observed in all three nozzles in Fig. 4a–c. They are also known as “ribs” in another elliptic jet study by Husain and Hussain (1993). Hence, for the sake of consistency during comparisons with their study, they will be known as ribs hereafter. Using inclined nozzle exits here distorts their formation asymmetrically as well as their subsequent interactions with the vortex roll-ups. No clear observation of any rib-like flow structures can be seen along the minor-planes. The ribs are formed when the vortex roll-ups accelerate towards the nozzle centerline and in the downstream direction, leaving behind slower jet fluid at opposite ends of the major-planes. These observations match the flow interpretations by Husain and Hussain (1993) and indicate that the formation of ribs remains robust despite the inclined nozzle exits. However, it can be

seen that inclined nozzles produce ribs which spread more outwards laterally than those for the reference nozzle. The extent of their outwards spreading also depends on whether they form along the shorter or longer nozzle lengths.

Visual evidences indicate that the ribs tend to spread outwards more along the shorter nozzle length than along the longer nozzle length as shown in Fig. 4c. The net result is that the jet spread is asymmetric with discernible veering towards the shorter nozzle length side. It is expected that mass entrainment behaviour and hence the mechanisms for the mutual interactions between the ribs and vortex roll-ups will be uneven and more convoluted than those predicted by Husain and Hussain (1993) at the two opposite locations along the major-planes. With respect to the minor-planes, it remains unclear to the author at this point the exact mechanisms leading to the gradual narrowing of the jet-spread. However, the inclined nature of the vortex roll-ups and their dissimilar interactions with the ribs are likely to be responsible.

3.2 Flow measurements

Figure 5 shows time-averaged vorticity maps obtained for all three nozzles along their major- and minor planes. For the reference nozzle shown in Fig. 5a(i), mean flow features expected of an elliptic jet along its major-plane can be observed readily. For instance, the formation of a "valley" due to the movement of the vortex roll-ups towards the nozzle centerline can be observed. Additionally, ribs are also observed to form in the symmetrical jet shear layers, similar to what was observed by Husain and Hussain (1993). On the other hand, vorticity contours along the major-plane depicted in Fig. 5a(ii) and (iii) clearly show asymmetric vorticity distribution for the 30° and 60° inclined nozzles. Interestingly, with the imposition of the inclined nozzle exits as shown in Fig. 5a(ii) and (iii), little or no evidence of valleys within the jet shear layers along the shorter nozzle lengths can be detected even though flow images shown earlier indicated their presence. In contrast, valleys can still be seen in jet shear layers along the longer nozzle lengths with corresponding downstream shifts, even though they recover slightly for the case of the 60° inclined nozzle. For example, valleys are observed to be located at approximately $x/D_h = 3$, 4.5 and 4.2 for the reference, 30° and 60° inclined nozzles, respectively. Hence, it can be deduced that the interactions between the ribs and vortex roll-ups (and thus entrainment) can be manipulated by the extent of the incline-angle.

On the other hand, corresponding vorticity maps shown in Fig. 5b demonstrate that there exist very little practical differences in the mean shear layer behaviour along the minor-plane despite the change in incline-angle. No valleys within the jet shear layers can be observed as well, thus signifies that no ribs are formed along the minor-planes. Between Fig. 5a and b, maximum vorticity plot levels along the minor-planes are discernibly higher than their counterparts along the major-planes. For instance, maximum vorticity levels for the reference, 30° and 60° inclined nozzles along the major-planes are 20.5, 21.0 and 20.3 s^{-1}, respectively. However, corresponding maximum vorticity levels along the minor-planes are 23.0, 24.1 and 23.0 s^{-1}, respectively. Ho and Gutmark (1987) observed that elliptic jet instabilities are associated with regions with maximum vorticity, which in turn is linked to the thinnest momentum thickness. Hence, the situation depicted in Fig. 5 is in good agreement with the earlier flow images, where rolling-up of the jet shear layer tends to occur along the minor-planes before anywhere else along the elliptic jet circumference. There are some small differences in the magnitudes of the vorticity levels between the three nozzles along the major- and minor-planes, respectively but they are not significant. Hence, the effect of varying the incline-angle here is to essentially distort the underlying interactions between the vortical structures and displace their regions of influence along the major-plane direction.

Clearly, accompanying these changes to the underlying vortex dynamics involving the vortex roll-ups and ribs will be variations in the mixing behaviour of the jet flows. Time-averaged streamwise, cross-stream and Reynolds shear stresses (i.e. normalised $u'u'$, $v'v'$, $u'v'$, respectively) are presented here to provide some insights into the mixing characteristics. However, it should be mentioned that due to the low Reynolds number flows and relatively small number of datasets used here, they should be treated as for first-hand comparison purposes here only. It has been shown previously by Hussain and Husain (1989) that elliptic jet behaviour is sensitive towards azimuthal momentum thickness variation, initial flow conditions as well as forcing amplitude, thus care needs to be taken when inferring the present findings to other flow situations. With that, Figs. 6, 7, and 8 compare the distributions of the three different flow stresses between the three nozzles along the major- and minor-planes. To ease comparisons, magnitudes of the maximum flow stresses for each nozzle along the shorter and longer nozzle lengths are summarised in Table 1. Note that the shorter and longer nozzle lengths for the reference nozzle refer to the corresponding physical regions as with the inclined nozzles for consistency.

Considering the distributions of the three flow stresses along the major-plane of the reference nozzle first, it can be noticed that they are clearly driven by the inwards movement and downstream acceleration of the vortex roll-ups along the major-plane as they switch their axes as shown in Figs. 6a(i), 7a(i) and 8a(i). In accordance to the motions of the vortex roll-ups, the flow stress distributions in the jet

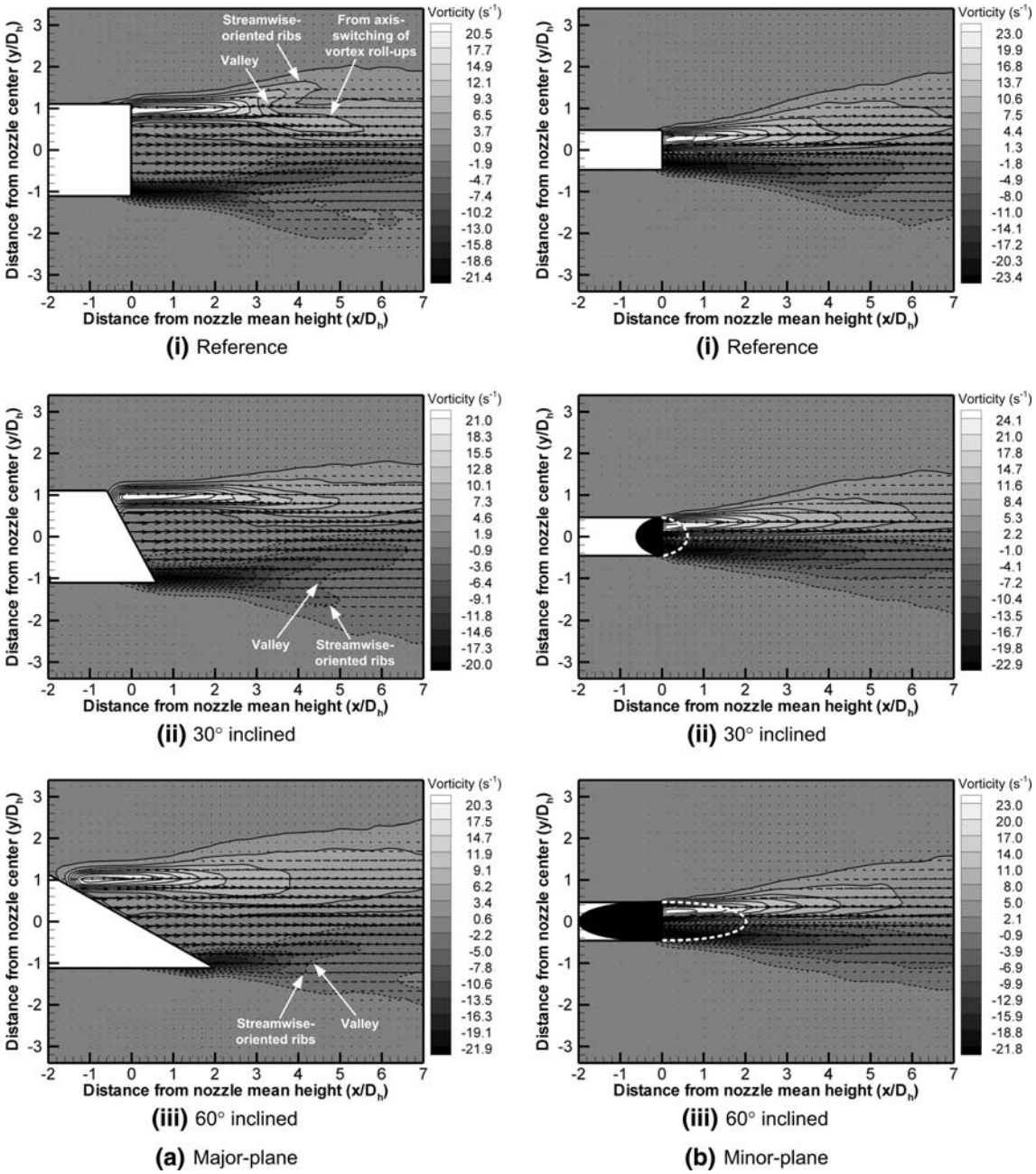

Fig. 5 Time-averaged vorticity maps for all three nozzles along their **a** major-planes and **b** minor-planes

shear layers along the major-planes depict increasing higher magnitudes towards the nozzle centerline with increasing downstream distance until approximately $x/D_h = 4$. One can also detect the influence of the typical axis-switching behaviour along the minor-planes on the flow stress distributions at $x/D_h = 2$ location in Fig. 6a(i) and 8a(i), where the vortex roll-ups along the minor-planes move outwards and away from the nozzle centerline. This leads to observable increases in the major-plane streamwise and Reynolds shear stresses. The contribution towards all the flow stresses by the ribs along the major-plane can be detected by the presence of valleys in the stress distributions where they are physically located, relatively similar to the vorticity maps shown earlier.

When inclined nozzles are used, Figs. 6a, 7a and 8a show that all three flow stress distributions along the major-planes become progressively more asymmetric as the incline-angle increases. At the maximum 60° incline-angle used here, all three flow stresses demonstrate significantly higher magnitudes along the longer nozzle lengths rather than along

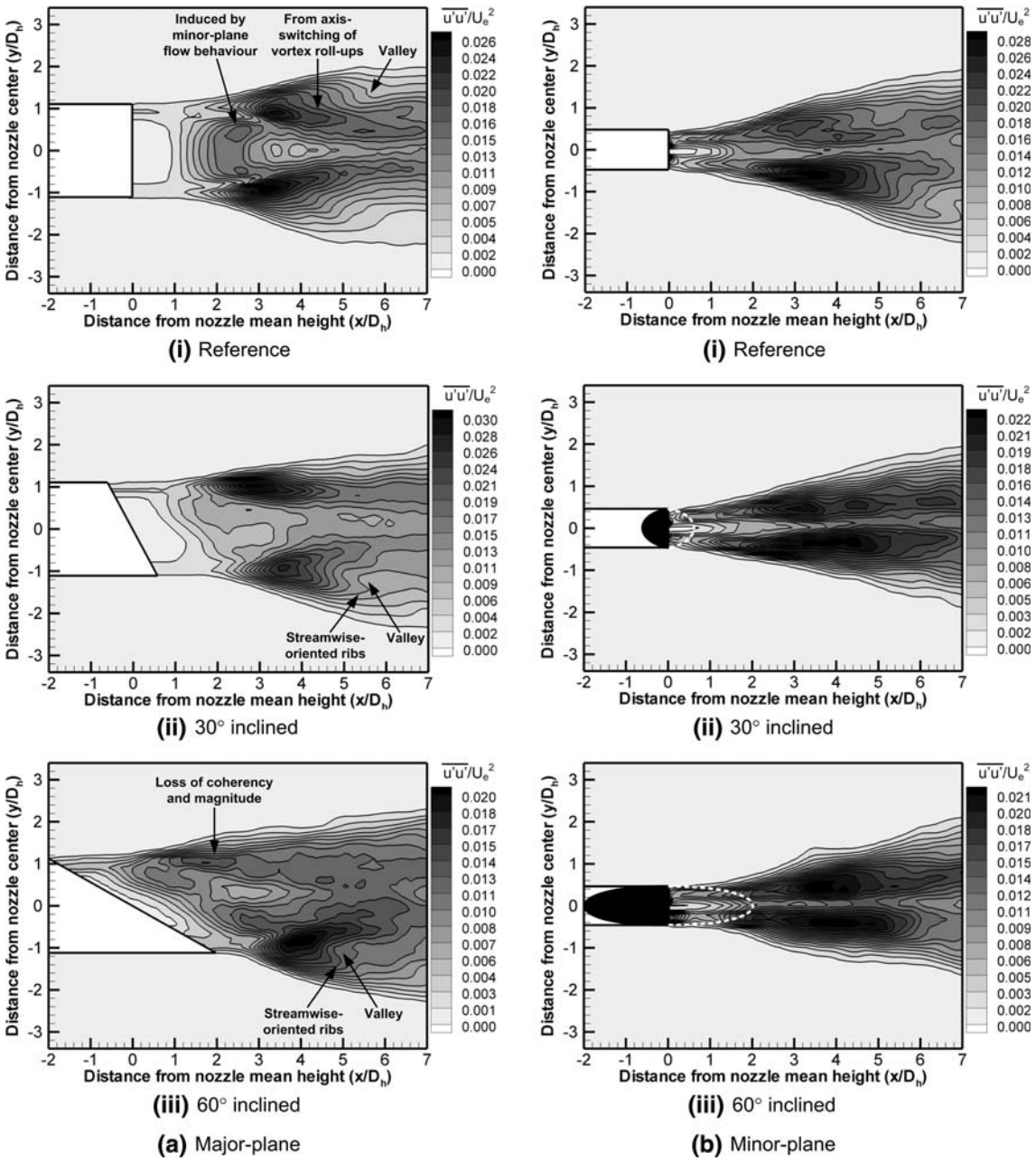

Fig. 6 Time-averaged streamwise flow stress distributions for all three nozzles along their **a** major-planes and **b** minor-planes

the shorter nozzle lengths. For example, the magnitudes of maximum normalised streamwise, cross-stream and Reynolds flow stresses are 0.014, 0.008 and 0.006, respectively along the shorter nozzle lengths. In comparison, corresponding maximum magnitudes along the longer nozzle lengths are 0.02, 0.017 and 0.009, respectively. Similar to the previous vorticity maps, no valleys or evidence of ribs can be found along the shorter nozzle lengths in the flow stress distributions for both inclined nozzles. Instead, valleys are clearly present in their stress distributions along the longer nozzle lengths, as indicated in the figures. In terms of the flow stress magnitudes, there is a slight increase in the maximum streamwise and Reynolds stress levels for the 30° inclined nozzle along the shorter nozzle length as compared to the reference nozzle. For instance, maximum normalised streamwise and Reynolds flow stress levels increase from 0.026 to 0.03 and 0.009 to 0.011, respectively when the 30° inclined nozzle was used. However, they reduce significantly along both nozzle lengths when the incline-angle was further increased to 60°.

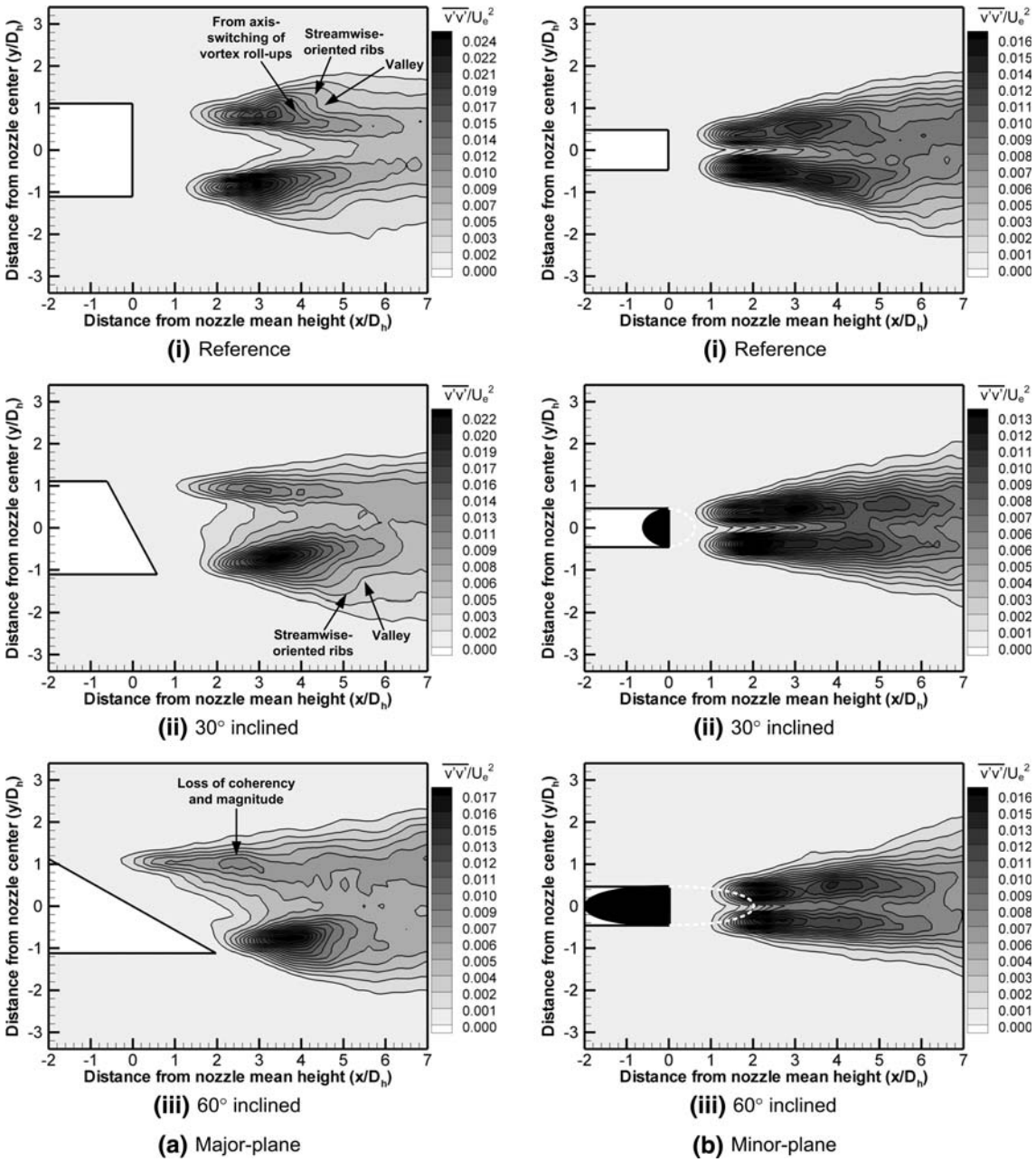

Fig. 7 Time-averaged cross-stream flow stress distributions for all three nozzles along their **a** major-planes and **b** minor-planes

Along the shorter nozzle lengths, the maximum normalised streamwise, cross-stream and Reynolds flow stress levels decrease from 0.03 to 0.014, 0.012 to 0.008 and 0.011 to 0.006, respectively. Similarly along the longer nozzle lengths, these corresponding flow stresses are observed to decrease from 0.026 to 0.02, 0.022 to 0.017 and 0.011 to 0.009 respectively.

As for the cross-stream flow stress levels, they consistently show reduction with increase in the incline-angle, along both the shorter and longer nozzle lengths. For example, along the shorter nozzle lengths, the maximum normalised cross-stream flow stress level reduces from 0.02 for the reference nozzle to 0.012 for the 30° inclined nozzle, before decreasing further to 0.008 for the 60° inclined nozzle. Correspondingly, along the longer nozzle lengths, the maximum normalised cross-stream flow stress level for the reference nozzle is 0.024, before it subsequently decreases to 0.022 and 0.017 for the 30° and 60° inclined nozzles, respectively. It can also be observed that flow stress distributions along the shorter nozzle lengths

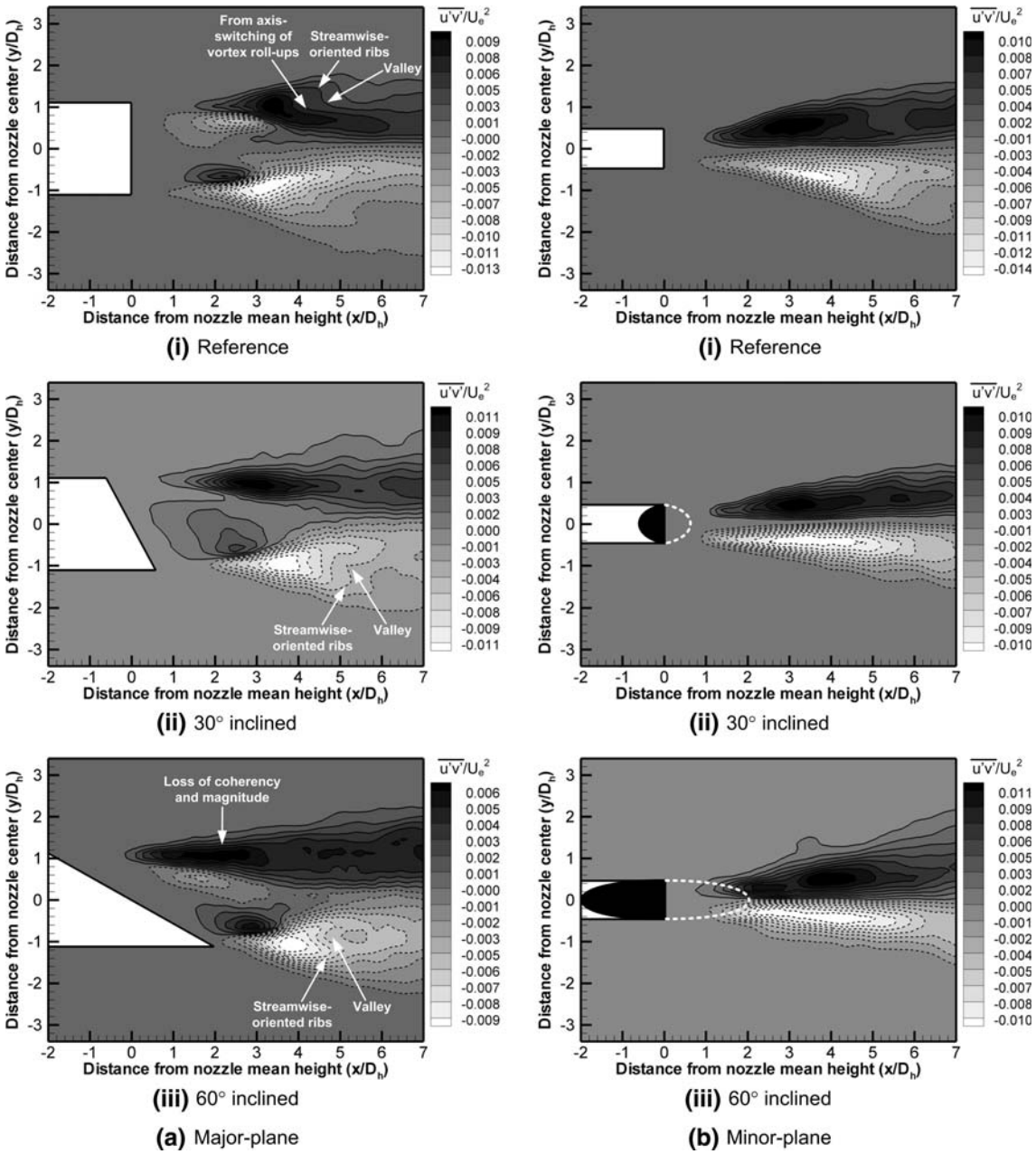

Fig. 8 Time-averaged Reynolds shear stress distributions for all three nozzles along their **a** major-planes and **b** minor-planes

gradually lose coherency during the increase in the incline-angle. On the other hand, those along the longer nozzle lengths retain much of their original coherency. One possible reason could be due to the rapid turning of the vortex roll-ups to re-orientate themselves from the inclined state to become perpendicular to the jet flow direction. It is conceivable that this behaviour disrupts the normal mixing characteristics along the shorter nozzle length. As for the three flow stress distributions shown in Figs. 6b, 7b and 8b, they are generally symmetrical about the nozzle centerline with little prominent flow features (for the sake of brevity, their detailed comparisons are not tabulated here and readers are referred to Figs. 6b, 7b, 8b). This is within expectations due to the fact that the incline-angle planes are along the major-planes of the elliptic nozzles rather than along its minor-planes. Hence, most significant flow differences arising from the use of inclined nozzles will logically be along the major-planes.

Analysis of the flow stress distributions above indicates that for the present flow configurations at least, the use of

Table 1 Summary of maximum normalised flow stress levels for each nozzle along the shorter and longer nozzle lengths along the major-plane

Nozzle type	Nozzle flow region	Streamwise stress ($u'u'/U_e^2$)	Cross-stream stress ($v'v'/U_e^2$)	Reynolds stress ($u'v'/U_e^2$)
Reference	Shorter length	0.026	0.020	0.009
	Longer length	0.026	0.024	0.013
30° incline	Shorter length	0.030	0.012	0.011
	Longer length	0.026	0.022	0.011
60° incline	Shorter length	0.014	0.008	0.006
	Longer length	0.020	0.017	0.009

inclined nozzles significantly affects mixing characteristics in terms of the flow stresses along the nozzle major-planes. To summarise, inclined nozzles systematically distort the axis-switching behaviour which in turn leads to generally more significant changes in flow stresses along the shorter nozzle lengths than along the longer nozzle lengths. With increasingly inclined vortex roll-up formations, the resultant flow field becomes increasingly strained. This leads to faster breaking down of not only the axis-switching behaviour, but the vortex flow structures as well. To further understand the source behind the redistribution of the flow stresses, Fig. 9 shows the distributions of the normalised turbulent kinetic energy levels for the three nozzles along the major- and minor-planes. They will reveal where the most energetic flow activities are taking place and their relative magnitudes.

Along both major- and minor-planes, it can be seen that the use of the elliptic inclined nozzles leads to a decrease in the maximum turbulent kinetic energy levels. For example, maximum normalised turbulent kinetic energy magnitude decreases from an initial 0.047 for the reference nozzle, to 0.043 and 0.036 for the 30° and 60° inclined nozzles, respectively along the major-planes subsequently. Similarly, corresponding magnitude along the minor-planes decreases from 0.042 to 0.033 as the incline-angle increases to 60°. Similar to the flow stress distributions covered earlier, inclined nozzles also lead to an increasingly asymmetric distribution along the major-planes here as the incline-angle increases. Furthermore, the distributions along the shorter nozzle length gradually lose strength and coherency until the longer nozzle length is associated with the maximum turbulent kinetic energy level with detectable coherency. Corresponding results along the minor-planes reveal symmetrical distribution of turbulent kinetic energy levels. This is not surprising, since earlier flow stress results have suggested such an outcome. These results indicate that when inclined nozzles are used and as the incline-angle increases, a shift in the spatial distribution of the vortical flow structures and their flow activities occurs. This is in good agreement with the flow images shown earlier.

In the study by Webster and Longmire (1997), they observed that circular inclined nozzles with significant incline-angles produce enhanced lateral spreading of axial momentum along both shorter and longer nozzle length regions. It will be interesting to see if a similar outcome can be achieved, although we need to be mindful of the differences in the underlying vortex dynamics between the two studies. Figure 10 shows the time-averaged normalised-velocity (i.e. U_m/U_e) contours determined for all three test nozzles along the major- and minor-planes. For the reference nozzle, Fig. 10a(i) shows that the potential core is clearly eroded by the strong presence of axis-switching behaviour in the reference nozzle. The adjacent contour lines also demonstrated a concerted narrowing of the jet column which limits the jet spread along the major-plane. As for the inclined nozzles, Fig. 10a(ii) and (iii) show that earlier initiation and subsequent development of the vortex roll-ups along the shorter nozzle lengths rather than the longer nozzle lengths result in asymmetric potential cores and jet spreads. However, as the flow continues to develop downstream, the differences between the two inclined nozzles reduce. On the other hand, Fig. 10b shows that the overall potential core and jet-spread behaviour along the minor-planes do not vary very significantly across the three nozzles. However, some slight narrowing of the jet column (which agrees with the flow images presented earlier) with the use of inclined nozzles as well as increase in incline-angle remains discernible. Lastly, the potential core length for the reference nozzle is estimated to be approximately $4D_h$, while those for the 30° and 60° inclined nozzles are approximately $3D_h$. Hence, the potential core length reduces by approximately one hydraulic diameter when inclined nozzles are used, as compared to the reference nozzle.

To further clarify the mean development of the jet columns, Fig. 11 compares the cross-stream velocity profiles along the major- and minor-planes for all three nozzles used here at $x/D_h = 1$ intervals. For the reference nozzle, it can be seen that the jet velocity profile along the major-plane is relatively uniform close to the nozzle exit. On the other hand, its counterpart along the minor-plane is significantly less uniform with a more parabolic distribution. The developments of the velocity profiles along the major- and minor-planes, respectively can be observed in Fig. 11a, where practically similar velocity profiles can be observed

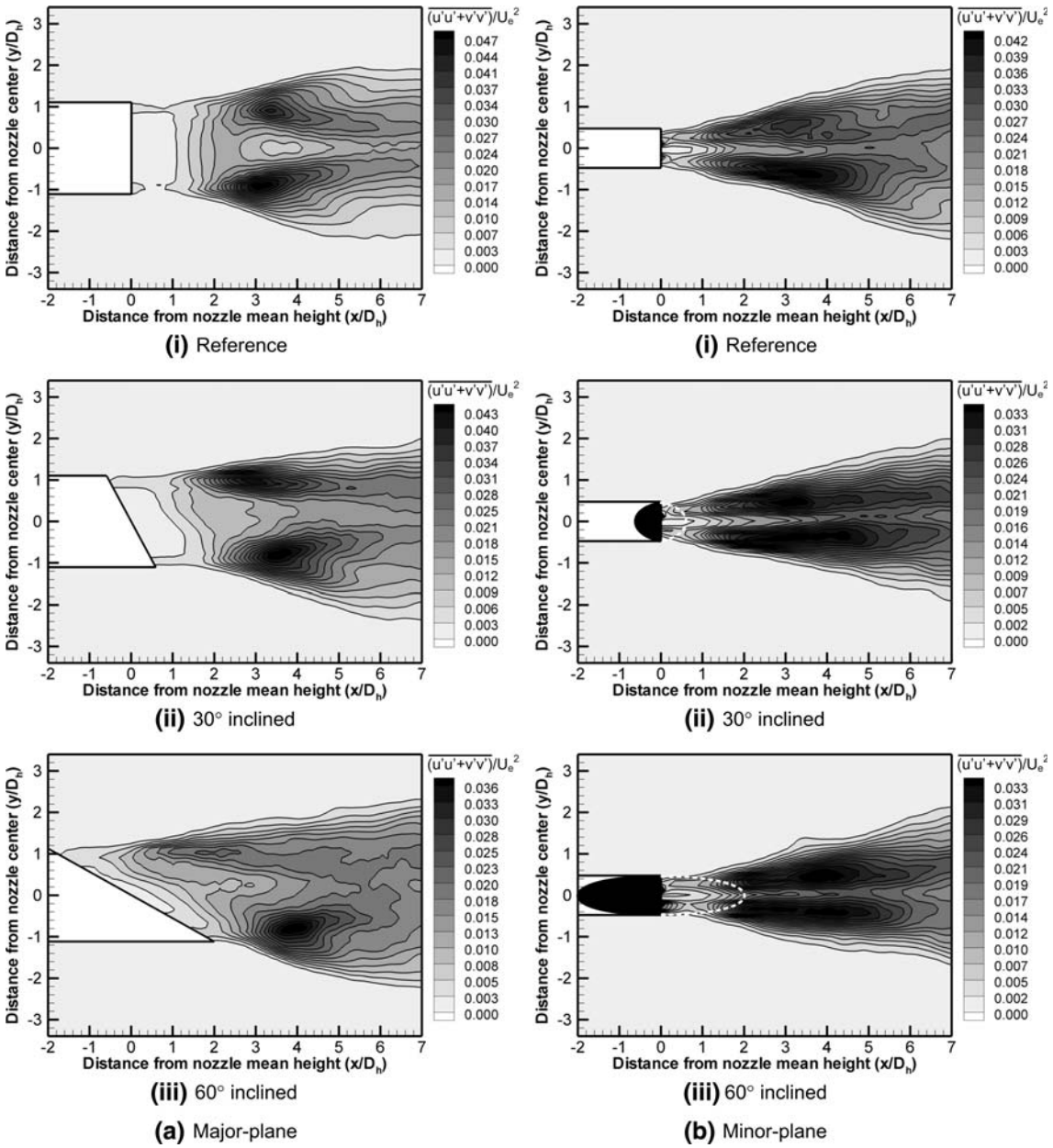

Fig. 9 Time-averaged turbulent kinetic energy distributions for all three nozzles along their **a** major-planes and **b** minor-planes

by $x/D_h = 7$. For the inclined nozzles shown in Fig. 11b and c, the results show that jet spreads along the major-planes are asymmetric. There exists a shift towards the shorter nozzle length sides and that the asymmetry increases with incline-angle. When the velocity profiles along the major-plane for the three nozzles are compared with one another (not shown here for brevity), they do not show any discernible increase in lateral jet-spread when inclined nozzles are used. This is in contrast to the case of circular inclined nozzles as observed by Webster and Longmire (1997). When similar comparison was carried out for the velocity profiles along the minor-plane, they are found to be almost similar with one another. It is worth noting from the figures that for the inclined nozzles, the discrepancy between the jet-spreads along the major- and minor-planes grows larger with increase in the incline-angle within the measurement range used here. From these results, it can be deduced that jet spread does not increase along either the shorter or longer nozzle lengths when elliptic inclined nozzles are used. Instead, the inclined nozzles lead to a gradual redistribution of the jet momentum towards the shorter nozzle length sides.

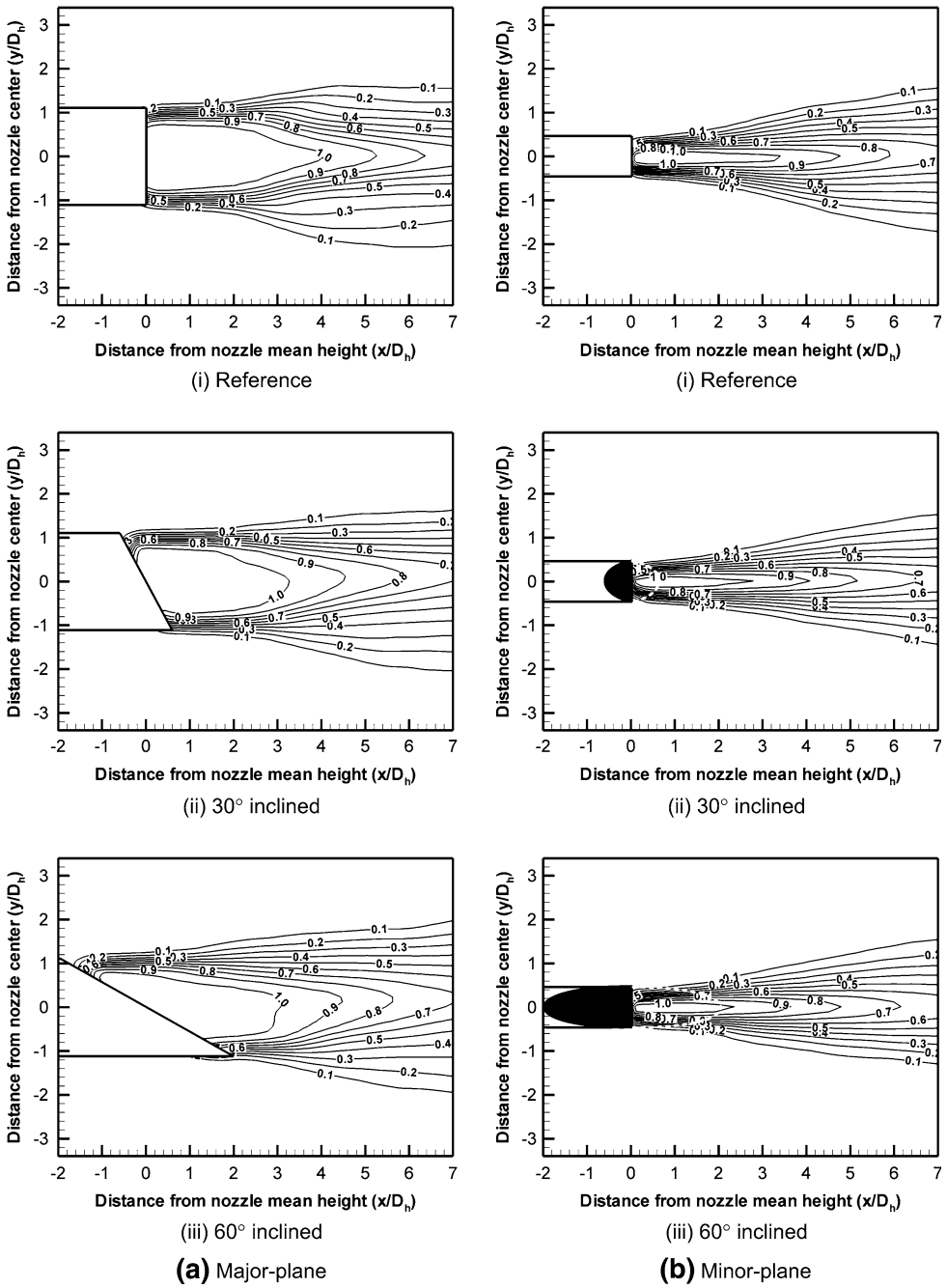

Fig. 10 Time-averaged normalised-velocity (U_m/U_e) contours of all three nozzles along their **a** major-planes and **b** minor-planes

Figure 12 shows typical instantaneous flow fields captured during DPIV measurements for the three nozzles along their major-planes. Compared to the earlier flow visualisation results, the formation of the dominant vortex structures and their subsequent behaviour are in good agreement. In particular, the production of the large-scale vortex roll-ups and the rib structures when the former surges towards the nozzle centerline can be seen here. These results also demonstrate that the jet columns do not possess clear serpentine-shaped outlines with the use of the inclined nozzles, in contrast to the observations made in Webster and Longmire (1997). Furthermore, the flow fields here are significantly more intense involving the productions and mutual interactions between flow structures with a multitude of length-scales. Collating all the evidence gathered thus far, one key reason is that the vortex roll-ups (along this plane) persistently move towards the nozzle centerline and transit to turbulence rapidly thereafter. Hence, the vortex roll-ups tend not to meander significantly. In the case of circular inclined nozzles with

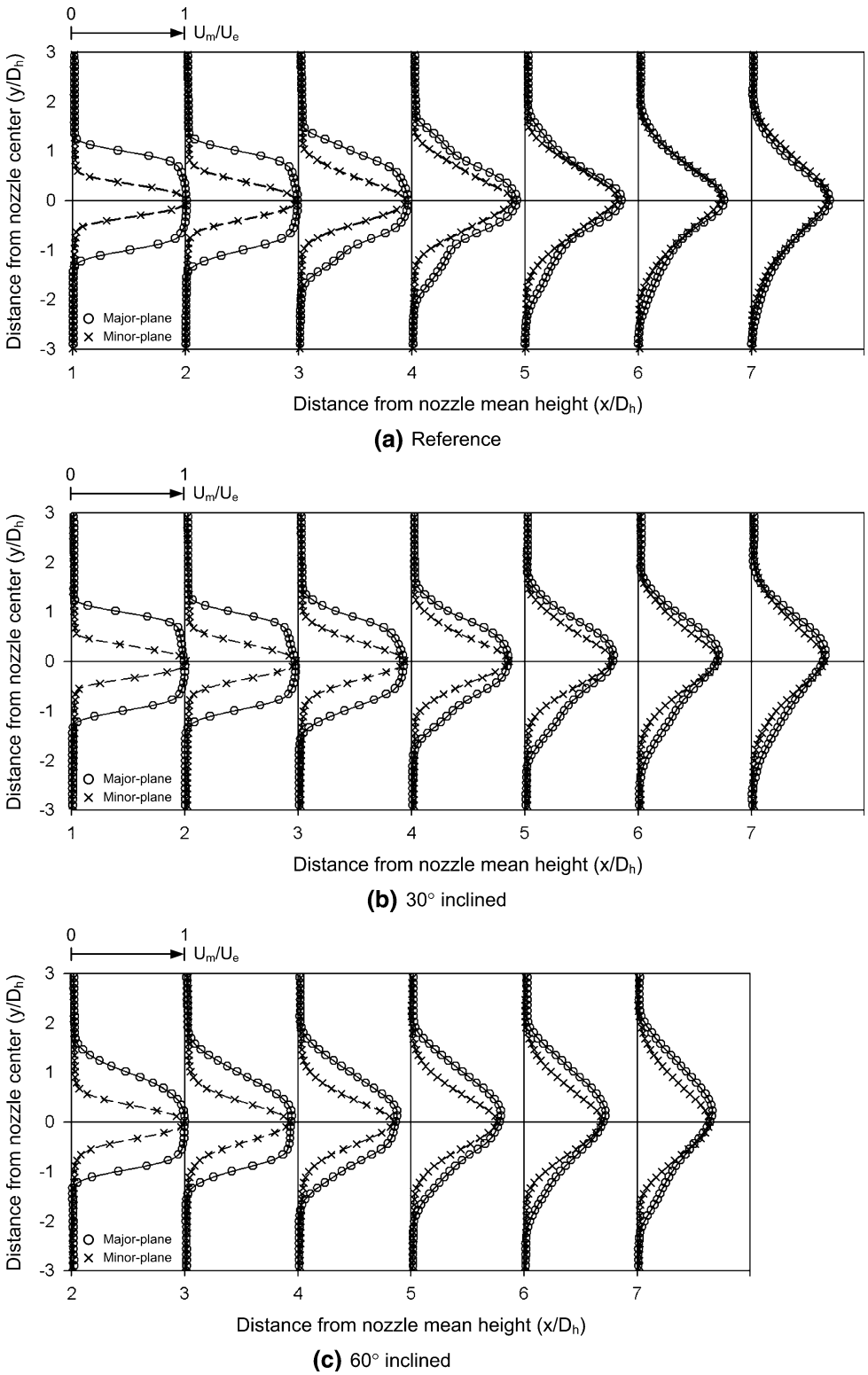

Fig. 11 Cross-stream velocity profiles along the major- and minor-planes for **a** reference, **b** 30° inclined and **c** 60° elliptic inclined nozzles

significant incline-angles, it is worth noting that the vortex roll-ups forming off the inclined nozzle exits will possess clear elliptic outlines. Hence, the distribution of vorticity (and hence self-induced velocities) along their circumferences will be different from a typical elliptic vortex ring. In that case, it is arguably plausible that the different levels of self-induced velocities along the vortex roll-ups cause the vortex roll-ups at the longer nozzle lengths to move towards the nozzle centerline along the major-plane, as depicted in Fig. 17 of Webster and Longmire (1997).

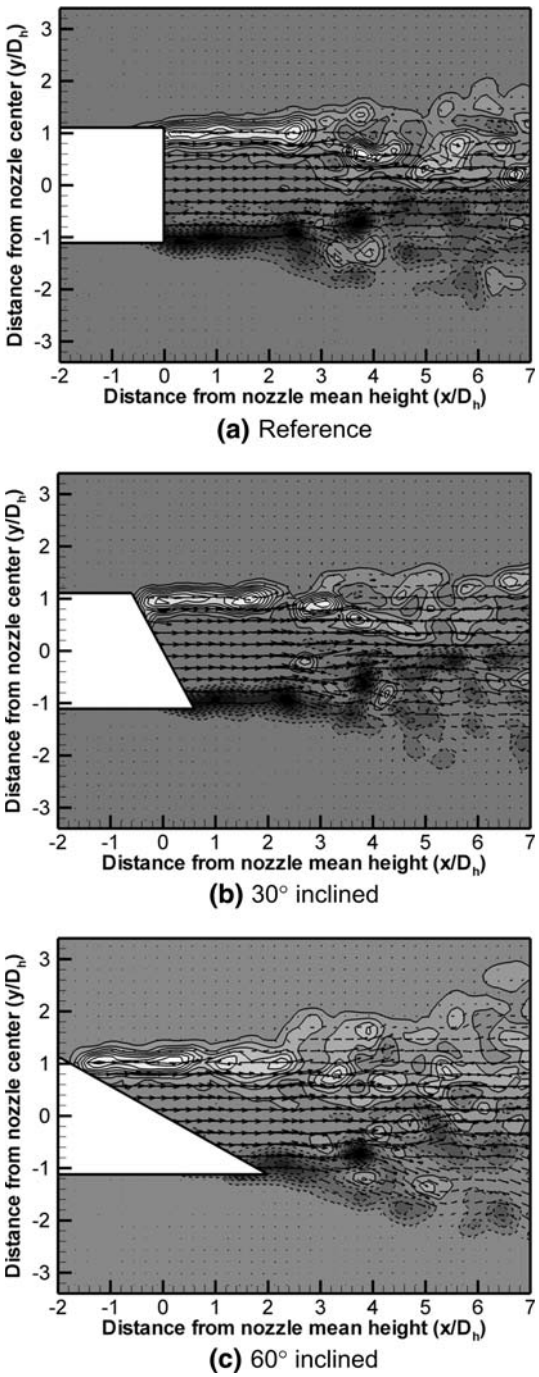

Fig. 12 Instantaneous vorticity maps captured for the **a** reference, **b** 30° and **c** 60° elliptic inclined nozzles

4 Conclusions

A study has been carried out on jets discharging from AR = 3 elliptic inclined nozzles under forced conditions. The aim is to investigate the effects of the inclined nozzle exits on the coherent vortex structures and associated time-averaged behaviour. Flow visualisation results show that for the elliptic reference nozzle, robust axis-switching behaviour exists under relatively low forcing amplitude. Shear layer instabilities manifest along the minor-planes before propagating towards the major-planes. When an elliptic inclined nozzle with moderate incline-angle (i.e. 30° incline) is used, it leads to jet shear layer instabilities and vortex roll-ups inclined parallel to the nozzle exit. The rolling-up of the jet shear layer initiates along the minor-planes, similar to elliptic reference nozzle though of lower intensity, and propagates faster towards the shorter nozzle length. Subsequent axis-switching is more limited with the overall alignment of the vortex roll-up remaining approximately parallel to the inclined nozzle exit.

When the incline-angle increases to 60°, initiation of vortex roll-ups is now associated with the shorter nozzle length rather than along the minor-plane, with the rolling-up process travelling towards the longer nozzle length. Although the jet shear layer instabilities are formed parallel to the inclined nozzle exit, subsequent developments of the vortex roll-ups result in a rapid re-orientation perpendicular to the jet flow direction. No axis-switching behaviour occurs for this particular inclined nozzle as the more convoluted vortex dynamics is observed to disrupt the normal flow processes significantly. Streamwise-aligned ribs are also observed in the flow images and their interactions with the vortex roll-ups become asymmetric with the use of inclined nozzles as well.

Time-averaged DPIV results show higher vorticity levels along the minor-planes rather than along the major-planes which agree well with previous observations by Ho and Gutmark (1987). Comparisons between the uses of inclined nozzles with the reference nozzle in terms of flow stresses reveal distributional changes to the mixing characteristics along the major-plane. In this case, their distributions become increasingly asymmetric with corresponding increase in the incline-angle. There is also a general reduction in the magnitudes and coherency of the flow stresses associated with the short nozzle lengths when the incline-angle is increased. On the other hand, flow stresses associated with the longer nozzle lengths retain much of their coherency and strengths. No significant changes to the flow stress distributions along the minor-planes of all three elliptic nozzles used here can be observed.

The distributions of the turbulent kinetic energy show that the asymmetric flow stress distributions correspond to asymmetric spatial shift in the vortical structures and associated flow activities. Velocity contours and cross-stream velocity profiles show that elliptic inclined nozzles demonstrate discernible asymmetric shift in the jet-spread towards the shorter nozzle lengths and that the shift increases with incline-angle. Lastly, lateral increase in jet-spread along the major-planes due to the use of inclined

nozzles is observed to be significantly lower than the case of circular inclined nozzles. It is believed to be linked to the non-serpentine-shaped jet columns, in contrast to circular inclined nozzles.

Acknowledgments The author gratefully acknowledges D. Tsovolos for his assistance in the flow visualisation and DPIV experiments and the Research Support Budget from the Department of Engineering at the University of Liverpool for the study.

References

Bernal LP, Roshko A (1986) Streamwise vortex structure in plane mixing layers. J Fluid Mech 170:499–525

Crighton DG (1973) Instability of an elliptic jet. J Fluid Mech 59:665–672

Crowe CT, Chung JN, Troutt TR (1988) Particle mixing in free shear flows. Prog Energy Combust Sci 14:171–194

Gutmark E, Ho C-M (1985) Near-field pressure fluctuations of an elliptic jet. AIAA J 23:354–358

Gutmark E, Ho C-M (1986) Visualization of a forced elliptic jet. AIAA J 24:684–685

Ho C-M, Gutmark E (1987) Vortex induction and mass entrainment in a small-aspect-ratio elliptic jet. J Fluid Mech 179:383–405

Husain HS, Hussain AKMF (1983) Controlled excitation of elliptic jets. Phys Fluids 26:2763–2766

Husain HS, Hussain F (1991) Elliptic jets. Part 2. Dynamics of coherent structures: pairing. J Fluid Mech 233:439–482

Husain HS, Hussain F (1993) Elliptic jets. Part 3. Dynamics of preferred mode coherent structures. J Fluid Mech 248:315–361

Husain HS, Hussain F (1999) The elliptic whistler jet. J Fluid Mech 397:23–44

Hussain F, Husain HS (1989) Elliptic jets. Part 1. Characteristics of unexcited and excited jets. J Fluid Mech 208:257–320

Keane RD, Adrian RJ (1992) Theory of cross-correlation analysis of PIV images. Appl Sci Res 49:191–215

Kinzie KW, McLaughlin DK (1999) Aeroacoustic properties of supersonic elliptic jets. J Fluid Mech 395:1–28

Lee SJ, Baek SJ (1994) The effect of aspect ratio on the near-field turbulent structure of elliptic jets. Flow Meas Instrum 5:170–180

Lim TT (1998) On the breakdown of vortex rings from inclined nozzles. Phys Fluids 10:1666–1671

Longmire EK, Duong LH (1996) Bifurcating jets generated with stepped and sawtooth nozzles. Phys Fluids 8:978–992

Morris PJ (1988) Instability of elliptic jets. AIAA J 26:172–178

New TH, Lim KMK, Tsai HM (2005) Vortical structures in a laminar V-notched indeterminate-origin jet. Phys Fluids 17:054108

Quinn WR (1989) On mixing in an elliptic turbulent free jet. Phys Fluids A 1:1716–1722

Schadow KC, Wilson KJ, Lee MJ, Gutmark EJ (1987) Enhancement of mixing in reacting fuel-rich plumes issued from elliptical jets. J Propuls Power 3:145–149

Tam CKW, Pastouchenko NN (2002) Noise from fine-scale turbulence of nonaxisymmetric jets. AIAA J 40:456–464

Webster DR, Longmire EK (1997) Vortex dynamics in jets from inclined nozzles. Phys Fluids 9:655–666

Webster DR, Longmire EK (1998) Vortex rings from cylinders with inclined exits. Phys Fluids 10:400–416

Wlezien RW, Kibens V (1986) Passive control of jets with indeterminate-origins. AIAA J 24:1263–1270